We are IntechOpen,
the world's leading publisher of
Open Access books
Built by scientists, for scientists

6,900
Open access books available

185,000
International authors and editors

200M
Downloads

154
Countries delivered to

Our authors are among the

TOP 1%
most cited scientists

12.2%
Contributors from top 500 universities

CLARIVATE ANALYTICS

BOOK CITATION INDEX

INDEXED

WEB OF SCIENCE™

Selection of our books indexed in the Book Citation Index
in Web of Science™ Core Collection (BKCI)

Interested in publishing with us?
Contact book.department@intechopen.com

Numbers displayed above are based on latest data collected.
For more information visit www.intechopen.com

Chapter

Using Clay-Gravel Mixtures as the Impervious Core Materials in Rockfill Dams

Zhongzhi Fu, Shengshui Chen, Enyue Ji, Guoying Li and Yang Lu

Abstract

Constructing the impervious system of an Earth Core Rockfill Dam (ECRD) usually needs a large volume of clay that may exhaust a huge area of farmland. One way to reduce the volume of clay to be filled is to use natural clay-gravel mixtures (CGM) or to add an appropriate percent of gravel materials into the clay and use the artificial clay-gravel mixtures as the impervious core materials. Using clay-gravel mixtures can also effectively increase the modulus of the core and reduce the differential settlement between the core and its adjacent rockfill shoulders, and thus alleviate the risk of occurrence of potential cracks within the core wall. The impermeability behavior of the compacted clay-gravel mixtures, however, has to be careful investigated and verified. In this chapter, four cases in using clay-gravel mixtures in constructing high ECRDs in China are reviewed, with attention focused on the engineering properties of clay-gravel mixtures and the construction and field quality control aspects of ECRDs using clay-gravel mixtures.

Keywords: rockfill dam, clay-gravel mixture, earth core, impermeability

1. Introduction

An Earth Core Rockfill Dam (ECRD) is a type of dam that uses a central or inclined clay core wall as the impervious system, while rockfill materials are used to construct the shoulders of the dam [1]. Information of some constructed high ECRDs around the world has been summarized by Zhang [2]. Normally, a good performance of an ECRD necessitates that the clayey soil used in its core meeting the following requirements [1, 3]: (a) The modulus of the compacted clay core should be high enough so that the arch effect between the core and the shoulders is not so evident as to result in horizontal cracks and hydraulic fracturing in the core. (b) The permeability of the clay core should be low enough so that the leakage after impounding does not exceed the expected quantity. Both requirements can be satisfied by proper gradation design and adequate compaction of the clayey soils used in the core wall [4].

In recent years, several high ECRDs have been constructed in western China and a common feature of these dams is the use of clay-gravel mixtures (CGM), either natural or artificially blended, as the impervious core materials. Control the mass content of gravel plays a central role in controlling the strength, deformation and permeability behavior of the mixtures obtained [2, 5]. For instance, increasing the

content of gravel results in an increase in the stiffness of CGM and is beneficial to reduce the differential settlement between the core and shoulders. On the other hand, the permeability also tends to increase as the content of gravel increases, which results in a potential risk of seepage failure and unacceptable leakage. A good design practice, therefore, needs a balance between the impermeability and deformation behavior. In this chapter, four cases of using CGM in constructing high ECRDs are reviewed, with particular attention focused on their engineering properties and the relevant construction concerns and field control tests.

2. Basic information of case studies

The four ECRDs considered are named PuBuGou (PBG) [5], ChangHeBa (CHB) [6–8], NuoZhaDu (NZD) [2, 9], and LiangHeKou (LHK) [10–12], respectively.

Dam		PBG	CHB	NZD	LHK
Height (m)		186	240	261.5	295
Reservoir volume (10^8 m^3)		53.37	10.75	237.03	107.67
Foundation	Type	Sand and gravel	Sand and gravel	Granite	Sandstone and slate
	Thickness (m)	78	79	-	-
Crest	Length (m)	540.5	497.9	630.1	650.0
	Width (m)	14	16	18	16
Dam slope (H:V)	Upstream	1:2.0 and 1:2.25	1:2.0	1:1.9	1:2.0
	Downstream	1:1.8	1:2.0	1:1.8	1:1.9
Core wall dimensions	Crest width (m)	4.0	6.0	10.0	6.0
	Bottom width (m)	96.0	125.75	114.6	150.0
	Ups. slope (V:H)	1:0.25	1:0.25	1:0.2	1:0.2
	Dws. slope (V:H)	1:0.25	1:0.25	1:0.2	1:0.2
Core wall materials	D_{max} (mm)	80	150	120	75
	$P\,(d < 5\,mm)$	39–54%	52–56%	60–70%	55%
	$P\,(d < 0.075\,mm)$	19–26%	26–29%	25–40%	28–44%
	$P\,(d < 0.005\,mm)$	3.6–8.3%	8–9%	≥8%	12–17%
	Permeability (cm/s)	≤10^{-5}	≤10^{-5}	≤10^{-5}	≤10^{-5}
	ρ_d/ρ_{dmax}	≥98%	≥97%	≥95%	≥97%
Filter thickness	Upstream (m)	4 m ×2	8 m ×1	4 m ×2	4 m ×2
	Downstream (m)	6 m ×2	6 m ×2	6 m ×2	6 m ×2
Seismicity	PGA (PE_{100} = 2%)	0.225 g	0.359 g	0.380 g	0.288 g
	PGA (PE_{100} = 1%)	0.268 g	0.430 g	0.436 g	0.345 g

Note: D_{max} = maximum particle diameter; d = diameter of soil particles; P = mass percentage of soil particles; ρ_d = dry density; ρ_{dmax} = maximum dry density; PGA = peak ground acceleration; PE_{100} = probability of exceedance within 100 years; 1g = 9.81 m/s^2.

Table 1.
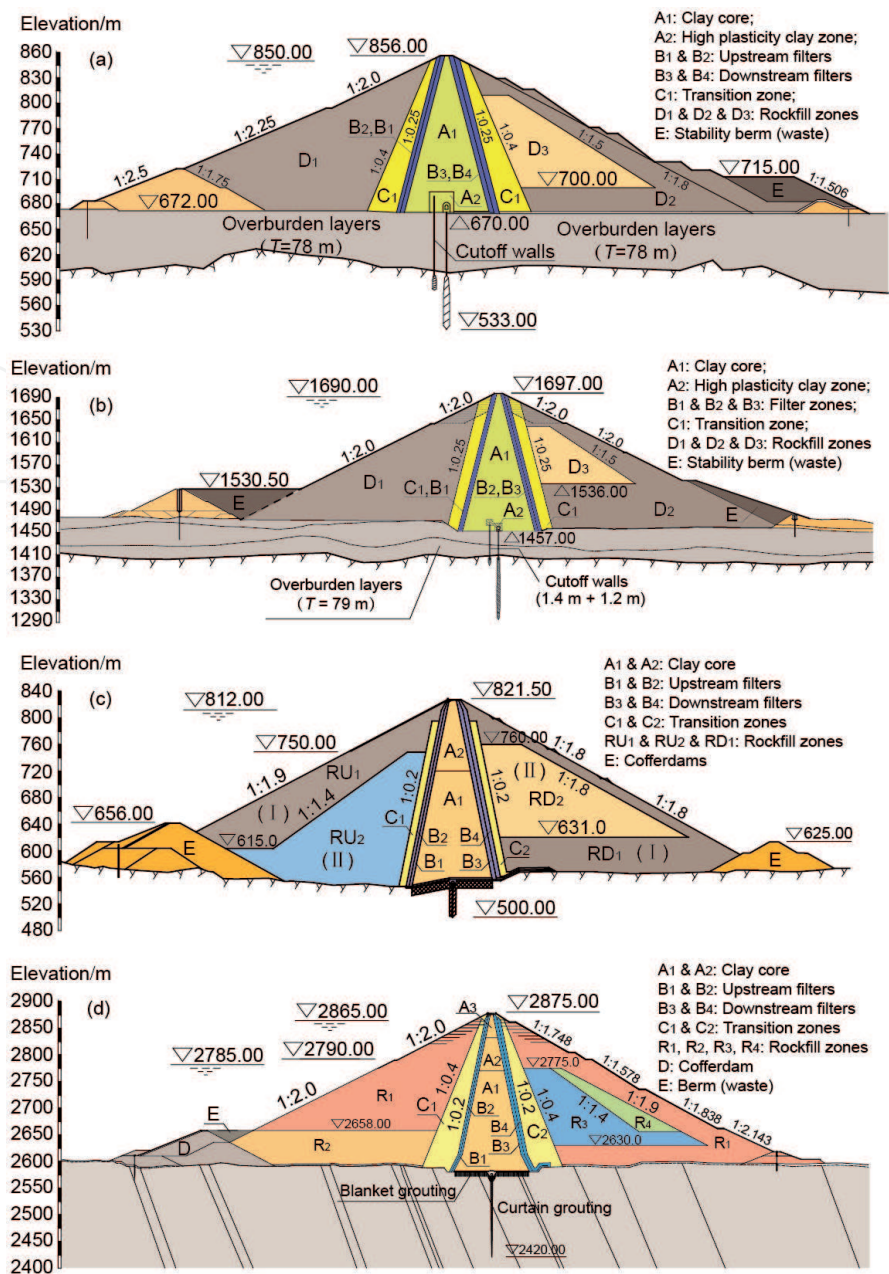*Basic information of the PBG, CHB, NZD and LHK ECRDs.*

Figure 1.
Material zones of the four ECRDs. (a) The PBG dam; (b) the CHB dam; (c) the NZD dam and (d) the LHK dam.

All four dams use central clay core walls, protected by filter zones upstream and downstream. PBG and CHB are ECRDs constructed over thick overburden layers with maximum depth of about 80 m, while NZD and LHK are seated on rock foundations. The basic information of the four dams are summarized in **Table 1** and their zones of materials are shown in **Figure 1**, respectively.

3. Properties of clay-gravel mixtures

3.1 Compaction characteristics

Laboratory compaction test is the most fundamental experiment performed in geotechnical engineering [13, 14], which provides the basis for determining the percent compaction and water content needed to achieve the required engineering properties, and for controlling construction to assure that the required compaction

and water content are achieved. For clay-gravel mixtures used in ECRDs, however, the existence of oversize fraction makes the two molds described by ASTM (with diameters of 101.6 mm and 152.4 mm, respectively) incapable of yielding reliable results. Therefore, special compaction molds with larger diameters were fabricated to establish the compaction curves. For instance, a modified compaction mold 500 mm in diameter was used for the PBG dam [5], and a mold with a diameter of 600 mm was fabricated for the NZD dam [2].

Figure 2 shows the influence of the mass percentage of soil particles larger than 5 mm (P_5) on the maximum dry density (ρ_{dmax}) and the optimum water content (ω_{opt}). Different compaction efforts were used for different cases. Note for the NZD dam P_5 was evaluated after compaction tests and for the rest three dams it was evaluated before compaction tests. Particle breakage may occur during compaction and the two approaches may give slightly different results. Nevertheless, common trends can be observed from **Figure 2**: an increase in P_5 from zero results in a steady increase in ρ_{dmax} until a threshold value is achieved, beyond which a further increase in P_5 leads to a rapid decrease in ρ_{dmax}. The value of this threshold is around 60–70% for the reviewed cases.

Corresponding to the different mass content of gravel particles, several states of clay-gravel structure can exist as illustrated in **Figure 3**, i.e., the state that gravel particles floating within the fine fraction, the state that gravel particles start to contact, and the state that fine fraction filling voids formed by gravel particles.
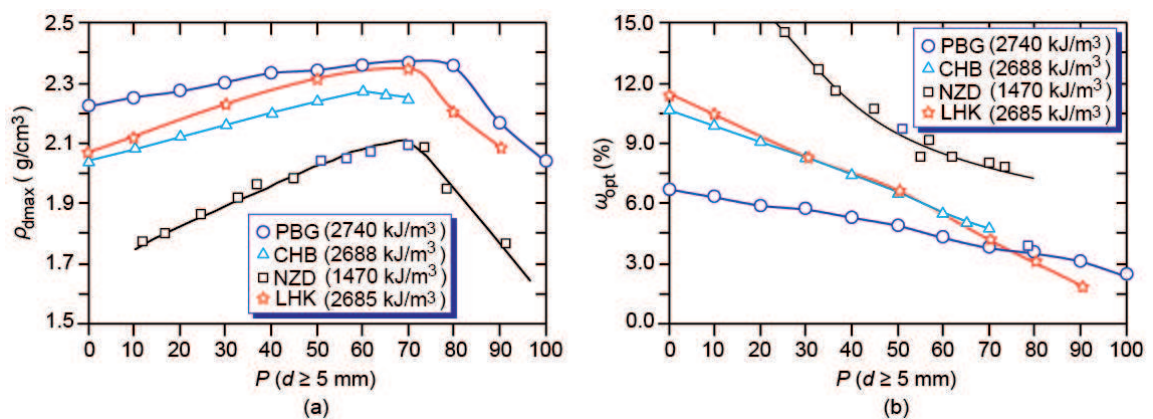

Figure 2.
Compaction test results on clay-gravel mixtures. (a) Maximum dry density and (b) optimum water content.
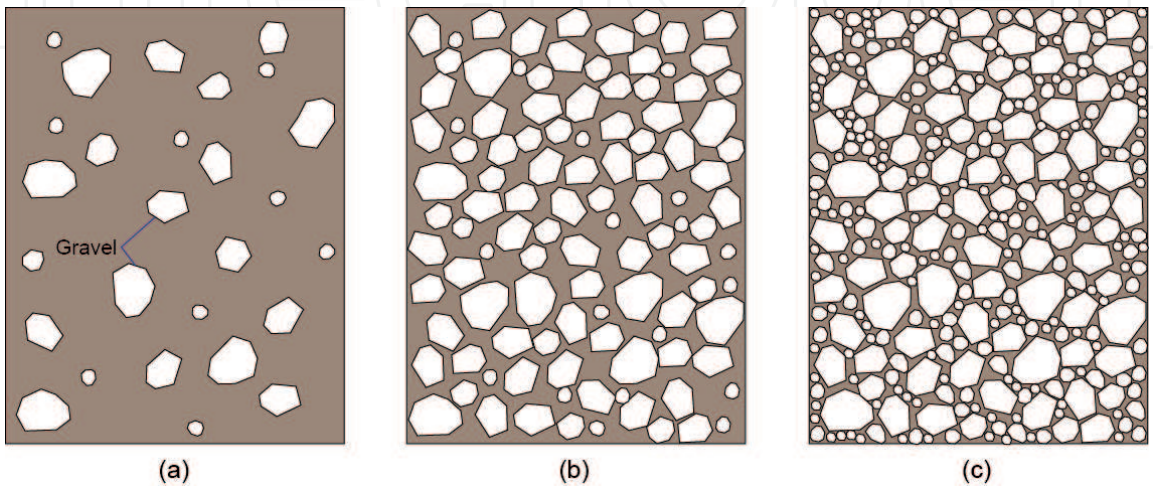

Figure 3.
Void filling characteristics of clay-gravel mixtures. (a) Skeleton formed by fine fraction, (b) skeleton formed by fine and gravel fractions, and (c) skeleton formed by gravel fraction.

In the first state the soil skeleton is formed by the fine fraction and the gravel particles seem to be floating within the soil matrix separately, i.e., only a very few or even no contacts are formed between gravel particles. In this case, the state of maximum dry density of the total material is achieved when the fine fraction itself is compacted to its maximum dry density. If we denote the maximum dry density of the fine fraction and the corresponding optimum water content by ρ^*_{dmax} and ω^*_{opt}, respectively, then the following theoretical relationship can be established for the maximum dry density of the total material (ρ_{dmax}):

$$\rho_{dmax} = \frac{\rho^*_{dmax} V_c + \rho_g V_g}{V_c + V_g} \tag{1}$$

in which ρ_g is the dry density of gravel particles. V_g and V_c denotes the total volumes of gravel particles and the fine fraction, respectively. The content of gravel, c_g, is defined as the mass of dry gravel divided by the total mass of the dry mixture, i.e.

$$c_g = \frac{\rho_g V_g}{\rho^*_{dmax} V_c + \rho_g V_g} \tag{2}$$

which can be rewritten as follows:

$$V_g = \frac{c_g}{1 - c_g} \frac{\rho^*_{dmax}}{\rho_g} V_c \tag{3}$$

Substituting Eq. (3) into Eq. (1) yields the following relationship:

$$\rho_{dmax} = \frac{\rho_g}{\left(1 - c_g\right)\rho_g + c_g \rho^*_{dmax}} \rho^*_{dmax} \tag{4}$$

It can be verified that $\rho_{dmax} = \rho^*_{dmax}$ when $c_g = 0$ and ρ_{dmax} increases with c_g when $\rho_g > \rho^*_{dmax}$. Various experiments have shown that the water content within the fine fraction is quite close to its optimum value (ω^*_{opt}) when the total material achieves its densest state [12, 15]. This conclusion can be used to establish the relationship between ω_{opt} and ω^*_{opt}, i.e.

$$\omega_{opt} = \frac{\rho^*_{dmax} V_c \omega^*_{opt} + \rho_g V_g \omega_g}{\rho^*_{dmax} V_c + \rho_g V_g} \tag{5}$$

in which ω_g denotes the water content of gravel particles when the CGM achieves a moisture equilibrium state and the fine fraction itself has a water content of ω^*_{opt}. Inserting Eq. (3) into Eq. (5) yields

$$\omega_{opt} = \left(1 - c_g\right)\omega^*_{opt} + c_g \omega_g \tag{6}$$

Obviously the optimum water content decreases almost linearly when the gravel content increases (**Figure 2**). In particular, the upper and lower bounds of ω_{opt} can be evaluated by setting ω_g to the water content that gravel particles are saturated but with dry surfaces and by setting it to zero, respectively.

As the mass content of gravel fraction ($d > 5$ mm) increases, the floating particles become increasingly close to each other and the theoretical threshold of this stage is that the gravel fraction achieves its loosest possible state, i.e., the particles just start to contact as shown in **Figure 3(b)**. In this state, the maximum void ratio of gravel fraction (e_{max}) can be expressed as follows:

$$e_{max} = V_c / V_g \tag{7}$$

Substituting Eq. (7) into Eq. (2) gives an empirical formula to estimate the upper bound of c_g that the floating pattern exist or the lower bound of c_g that the floating pattern starts to disappear, i.e.

$$c_g = \frac{\rho_g}{\rho_{dmax}^* e_{max} + \rho_g} \tag{8}$$

If the mass content of gravel fraction is further increased beyond the threshold given by Eq. (8), the soil skeleton will be formed by both the fine fraction and the gravel fraction. A higher c_g means a greater contribution made by the gravel fraction to the skeleton. In this case, the gravel fraction can be accommodated only by compacting the fine fraction to a looser state than the densest state, i.e., the fine fraction cannot be compacted to its densest state anymore. Correspondingly, Eq. (4) can be revised as follows:

$$\rho_{dmax} = \frac{\rho_g}{\left(1 - c_g\right)\rho_g + c_g \rho_d^*} \rho_d^* \tag{9}$$

in which ρ_d^* denotes the dry density of compacted fine fraction. Two competitive trends are implicated in Eq. (9). For a given ρ_d^*, an increase in c_g still leads to an increase in ρ_{dmax}. However, the increase in c_g meanwhile results in a decrease of ρ_d^*. The combined effect is that the ρ_{dmax} of the total material continues to increase when c_g is increased, with, however, a different trend from the previous stage. A peak for ρ_{dmax} is achieved at a particular c_g, exceeding which the value of ρ_{dmax} decreases rapidly as shown in **Figure 5**. In this stage, the total material is still easiest to compact when the water content of its fine fraction is ω_{opt}^*. It is easy to verify that Eq. (6) still holds.

The compaction characteristics can also be investigated from another extreme case that $c_g = 1$, i.e., the soil skeleton is completely formed by the gravel fraction. If the minimum void ratio of gravel fraction achievable after compaction is denoted by e_{min}, then the maximum dry density of the gravel fraction (total material in this case) reads:

$$\rho_{dmax} = \frac{\rho_g}{\left(1 + e_{min}\right)} \tag{10}$$

Adding a few amount of fine fraction will not change the soil skeleton, and the fine fraction is simply filling the inter-gravel voids. The dry density of the total material can then be expressed as follows:

$$\rho_{\text{dmax}} = \frac{\rho_d^* V_c + \rho_g V_g}{V_g (1 + e_{\text{min}})} \tag{11}$$

Because the compaction effort cannot be imparted to the fine fraction in this state, ρ_d^* can be interpreted as its dry density under uncompacted state. Inserting Eq. (3), with ρ_{dmax}^* replaced by ρ_d^*, into Eq. (11) yields

$$\rho_{\text{dmax}} = \frac{\rho_g}{c_g (1 + e_{\text{min}})} \tag{12}$$

It is clear that an increase of clay content (decrease of c_g) results in an increase in ρ_{dmax}, and the threshold can be attained when all the voids are filled by fine fraction, i.e., $V_c = e_{\text{min}} V_g$. In this case, Eq. (11) can be rewritten in the following form:

$$\rho_{\text{dmax}} = \frac{\rho_d^* e_{\text{min}} + \rho_g}{(1 + e_{\text{min}})} \tag{13}$$

Similar as Eq. (8), the threshold gravel content for this stage reads:

$$c_g = \frac{\rho_g}{\rho_d^* e_{\text{min}} + \rho_g} \tag{14}$$

Since the fine fraction is not compacted in this state, the optimum water content of the total material (ω_{opt}) has nothing to do with that of the void-filling fine fraction (ω_{opt}^*).

If the content of fine fraction is further increased beyond the threshold given by Eq. (14), it will start to participate in forming the soil skeleton, and a lower c_g means a greater contribution made by the fine fraction. In this case, some compaction effort is imparted to the fine fraction and the gravel fraction cannot be densified to e_{min} anymore. Eq. (9) has already been established to describe the compaction behavior for this state. A decrease in c_g results in a less compacted structure for the gravel fraction. On the other hand, the decrease in c_g also leads to an increase in ρ_d^*. The influence of c_g on ρ_{dmax} depends on the two competitive effects. **Figure 4** depicts the compaction behavior of clay-gravel mixtures in three states.

3.2 Permeability

It is important to verify that the impermeability of the compacted CGM meets the requirement of the design code. The permeability coefficient of the clay core is usually controlled below 10^{-5} cm/s [1]. **Figure 5** shows the influence of gravel content on the permeability coefficient. The seepage experiments on the material for the LHK dam is performed by Lu with a low percent compaction so
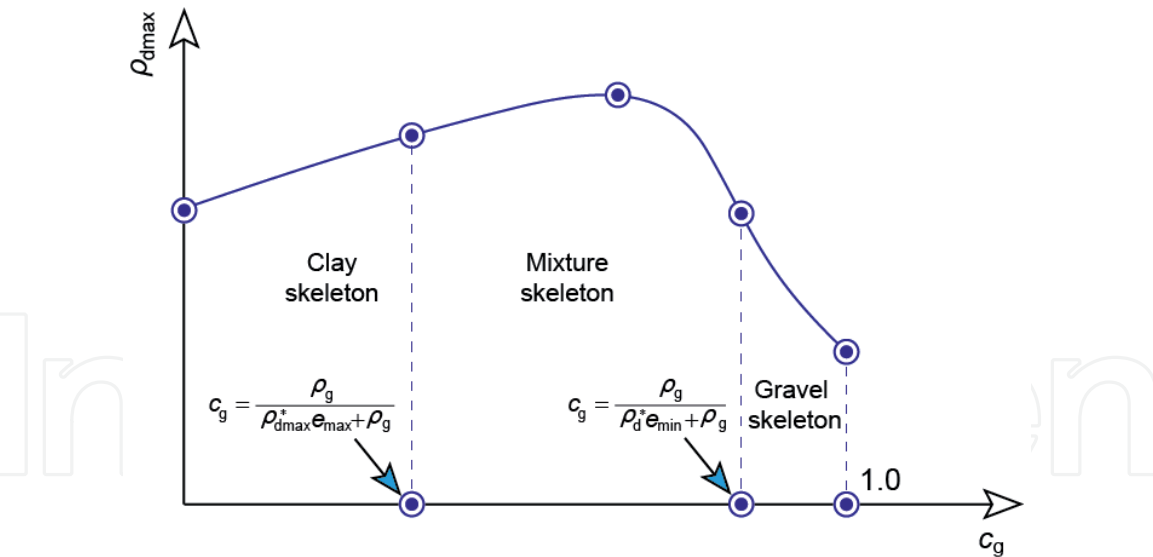
Figure 4.
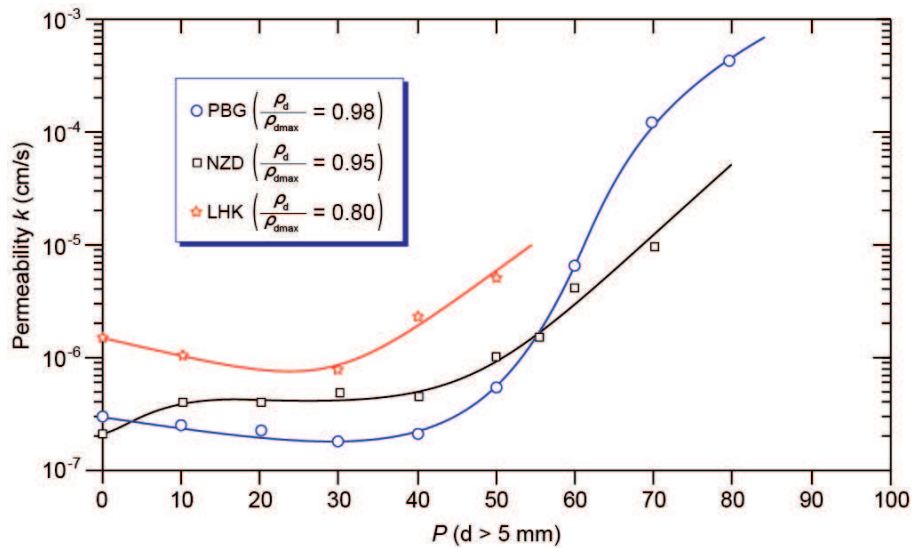*Influence of c_g on ρ_{dmax} in three skeleton states.*

Figure 5.
Influence of gravel content on the permeability.

that particle breakage was expected not evident [12]. A common feature of the approximating curves in **Figure 5** is the almost constant or a slight decrease of the permeability when the gravel content (P_5) is increased from zero to about 30%. The lowest permeability can be achieved when P_5 is around 30%. Beyond this amount, the permeability coefficient increases rapidly with a further increase in P_5.

Abundant double-ring infiltrometer tests were performed during test filling of the CGM used in the PBG dam [5]. The rate of vertical infiltration (k_v) is plotted against the dry density (ρ_d) and gravel content (P_5) in **Figure 6**. The results are rather scattered, indicating the inhomogeneous nature of the filled materials. However, it is clear that the places where the rates of infiltration are relatively high ($k_v > 10^{-5}$ cm/s) are either not well compacted with a relatively low density or have relatively high gravel contents. Therefore, it is important to control the gravel content below a certain limit to ensure the impermeability of the compacted CGM. When the CGM is in a mixture skeleton state (**Figure 4**), embedding an increased amount of gravel particles leads to a decreased percent compaction of the fine

fraction as pointed out previously. This tends to increase the permeability of the mixture. On the other hand, the embedded particles serve as seepage barriers as the permeability of gravel particles is considerably lower than the fine fraction. These two competitive effects control the dependence of the permeability of the total material upon the gravel content. Note that the rate of infiltration obtained in situ could not be used to determine the coefficient of permeability directly although both quantities have the same dimension [16].

Initial water content also has an influence on the permeability of compacted CGM. **Figure 7** shows typical results obtained from laboratory experiments with PBG CGM [5]. For a given grain size distribution and water content, the coefficient of permeability (k) decreases when the dry density of the total material is increased. However, the rate of decrease in permeability also decreases when the dry density is increased, indicating an increasingly difficulty in reducing the permeability. For the given compaction effort applied, the maximum dry density of the total material was achieved when ω = 4.625%. However, the permeability coefficient does not reach the minimum at this optimum water content: compacting the CGM slightly
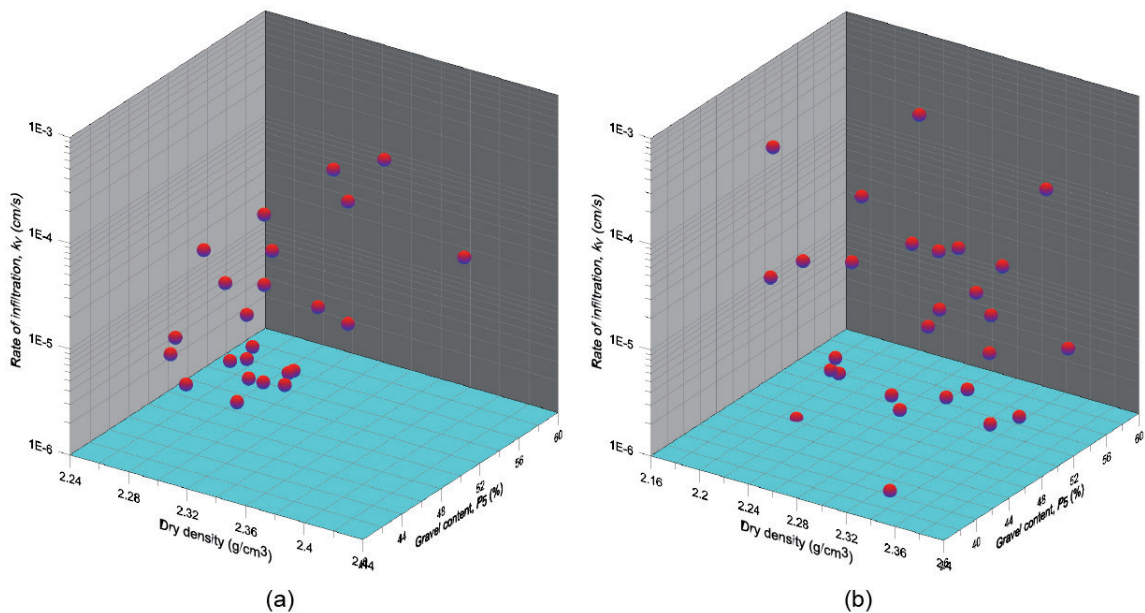

Figure 6.
Rate of infiltration measured during test compaction (PBG dam). (a) Lift thickness = 30 cm and (b) lift thickness = 40 cm.
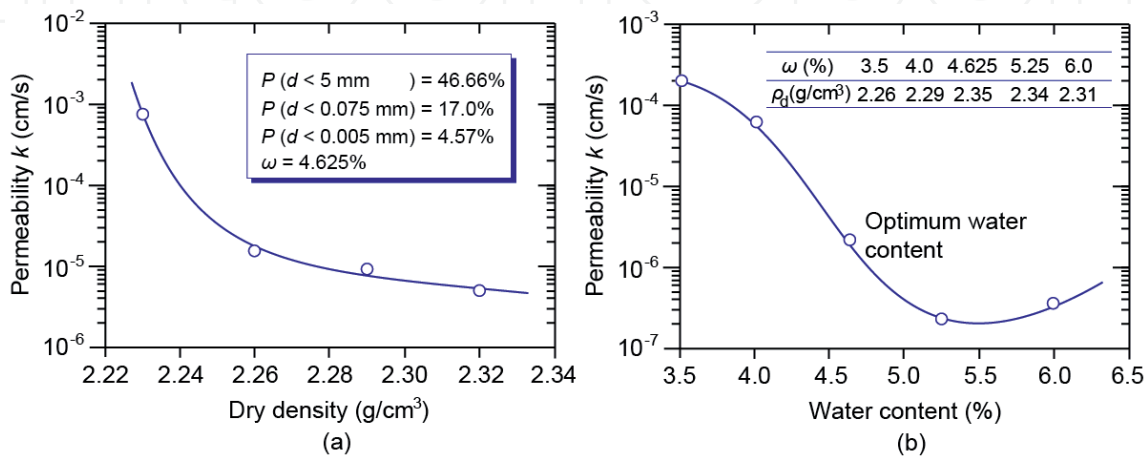

Figure 7.
Influence of dry density and water content on permeability. (a) Influence of dry density and (b) influence of water content.

wet of optimum results in a lower permeability although the resultant dry density is also lower than the maximum one (**Figure 7(b)**). It has been recognized very early that a dispersed microstructure (with a high degree of particle orientation) can be obtained for clay when it is compacted on the wet side (wetter than optimum) while compacting the same clay drier than optimum generally yields a flocculated microstructure (with a low degree of particle orientation) [17]. **Figure 8** replots the contours of permeability of a silty clay compacted by kneading action [18]. The lower permeability on the wet side than that on the dry side can be clearly observed from the distribution of contours.

Permeability is a good parameter indicating the pore structure. Since 1970s, the use of scanning electron microscopy and mercury intrusion porosimetry have shed sufficient light on the fabric of compacted clay [19]. It has been found that samples compacted dry of optimum tend to have a marked double-porosity fabric, with a macro-fabric consisting of large clay packets or macropeds separated by inter-packet voids as demonstrated in **Figure 9**. Samples compacted wet of optimum, on the other hand, have a relatively uniform fabric [20]. Therefore, dam CGM is better to be compacted slightly wetter than optimum. Another important benefit of compacting CGM wet of optimum is the less amount of wetting-induced collapse upon saturating during reservoir impounding [19, 20].
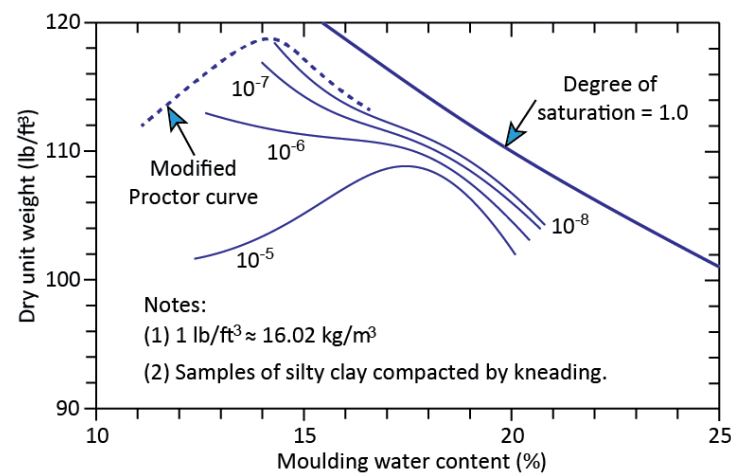

Figure 8.
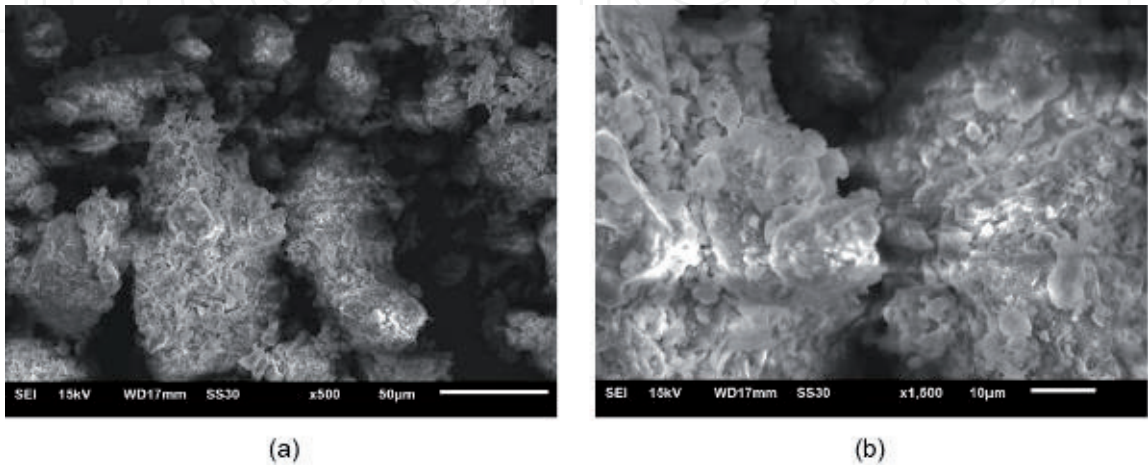*Contours of permeability under saturated condition. From Mitchell et al. [18].*

Figure 9.
Double-porosity fabric of the clay used in the LHK ECRD. (a) Amplified 500 fold and (b) amplified 1500 fold.

3.3 Strength

Two aspects of strength of CGM deserve attention in designing, i.e., the shear strength and the tensile strength. The shear strength is important for slope stability analyses and the tensile strength is useful in estimating the possibility of cracking under various conditions. The authors tested the CGM used in the CHB dam and investigated the influences of the gravel content on the strength components, i.e., the cohesion (c) and the friction angle (φ). The results are shown in **Figure 10**. Note each soil specimen was compacted to its maximum dry density under its optimum water content. The cohesion decreases steadily as a result of an increase in gravel content. On the contrary, the friction angle increases when the gravel content is increased. The CGM changes from a cohesive soil to a granular soil when the gravel content is gradually increased.

Uniaxial tensile experiments were also performed for the CHB CGM specimens with different gravel contents, and the typical results are shown in **Figure 11**.
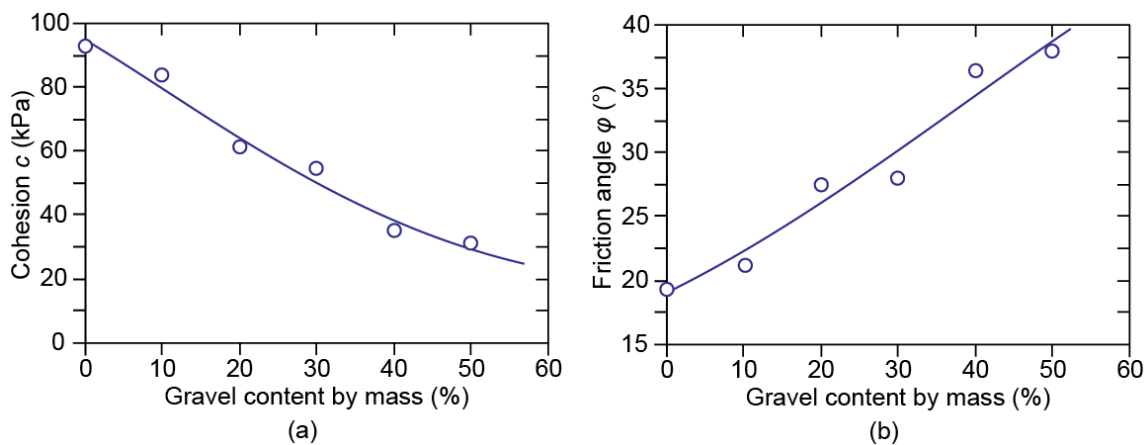

Figure 10.
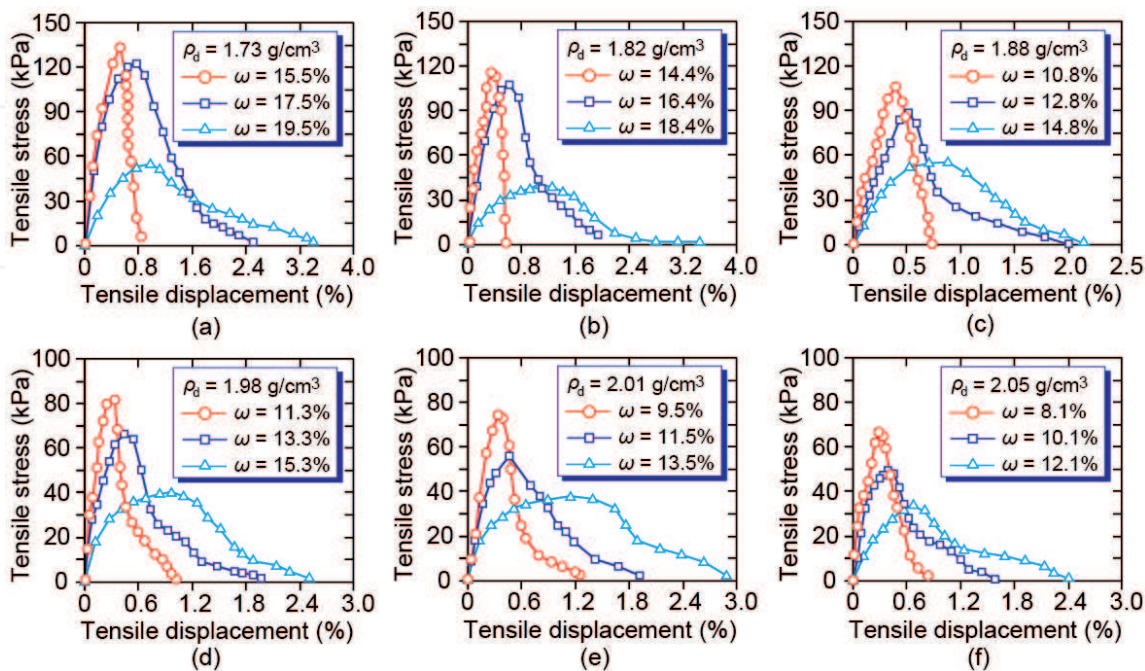*Influence of gravel content on the shear strength. (a) Cohesion and (b) friction angle.*

Figure 11.
Tensile strength of CGM with different gravel content. (a) c_g = 0, (b) c_g = 10%, (c) c_g = 20%, (d) c_g = 30%, (e) c_g = 40%, (f) c_g = 50%.

For each gravel content, three different water contents were considered, i.e., ω_{opt}-2%, ω_{opt}, and ω_{opt}+2%. Variation of water content may occur as a result of sun exposure, rainfall or fluctuation of reservoir level. It can be seen in **Figure 11** that the tensile strength of CGM decreases significantly when the water content is increased. This is not surprise because matric suction of the unsaturated CGM contributes to its tensile strength and a wetter state indicates a lower matric suction. Despite of the higher strength of drier specimens, the tensile displacement corresponding to the peak tensile strength decreases when the water content is reduced, indicating an increasingly brittle response of specimens dry of optimum and increasingly ductile responses of specimens wet of optimum. **Figure 11** also shows that when the gravel content is increased from zero to 50% tensile strength of specimens compacted to their densest states at their optimum water contents decreases gradually from 123 kPa to 50 kPa. These results indicate that CGM with a higher gravel content is more prone to crack, particularly when it is in a dry state.

3.4 Deformation

The deformation characteristics of CGM are generally studied by consolidated and drained triaxial compression experiments. **Figure 12** shows some typical stress vs. strain and volume change results obtained for CGMs used in the NZD and LHK dams. Strain-hardening behavior can be observed for both materials, particularly under a high confining pressure, e.g., when the confining pressure is over 2.0 MPa peak deviatoric stress cannot be attained even when the specimen is sheared to an axial strain of 15% as shown in **Figure 12(b)**. The volumetric response is generally contractive. However, shear dilation can present when the confining stress is low as illustrated in **Figure 12(a)**.

The general trends shown in **Figure 15** indicate that the deformation behavior of CGM can be well described by the constitutive model proposed by Duncan and Chang [21]. The model is based on a hyperbolic relationship between the deviatoric stress and the axial strain, and the tangential modulus (E_t) depends on the stress state including the minor principal stress (σ_3) and the stress level, i.e.

$$E_t = \left[1 - R_f \frac{(1-\sin\varphi)(\sigma_1 - \sigma_3)}{2c\cos\varphi + 2\sigma_3\sin\varphi} \right]^2 \cdot k \cdot p_a \cdot \left(\frac{\sigma_3}{p_a} \right)^n \tag{15}$$

in which σ_1 denotes the major principal stress and p_a the atmospheric pressure. c and φ are shear strength parameters. R_f, k and n are three modulus parameters.

The axial strain and the radial strain can also be assumed following a hyperbolic relationship, which yields the final representation of the tangential Poisson ratio (ν_t) as follows [21]:

$$\nu_t = \frac{G - F\lg\left(\dfrac{\sigma_3}{p_a}\right)}{\left\{ 1 - \left[1 - R_f \dfrac{(1-\sin\varphi)(\sigma_1 - \sigma_3)}{2c\cos\varphi + 2\sigma_3\sin\varphi} \right]^{-1} \cdot \dfrac{D \cdot (\sigma_1 - \sigma_3)}{k \cdot p_a \cdot (\sigma_3 / p_a)^n} \right\}^2} \tag{16}$$

in which G, F, and D are another three parameters. **Table 2** summarizes the model parameters of the CGM used by different authors for the reviewed four dams. They may be used as references when similar cases are encountered.
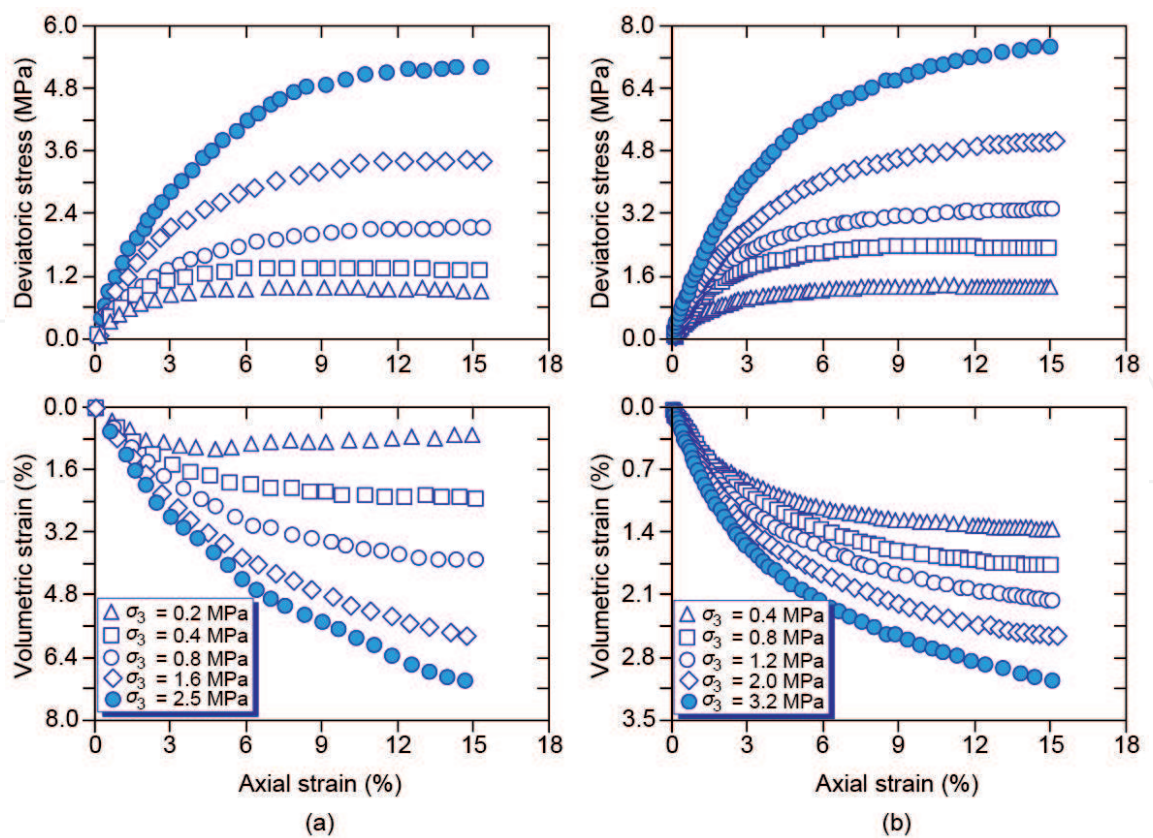
Figure 12.
Results of drained triaxial experiments on typical CGM. (a) CGM in the NZD dam and (b) CGM in the LHK dam.

Parameters	R_f	k	n	G	F	D	φ (°)	c (kPa)	ρ_d (g/cm³)	Reference
PBG	0.78	550	0.31	0.31	0.07	4.0	34.0	60.0	2.36	[5]
	0.76	550	0.42	0.39	0.01	7.5	35.0	12.0	2.30	
CHB	0.87	646	0.40	0.40	0.04	2.0	31.1	12.0	2.22	[22]
	0.86	473	0.32	0.43	0.06	1.4	23.9	50.0	2.19	
NZD	0.63	405	0.47	0.31	0.04	5.9	33.0	60.0	1.93	[2]
	0.76	415	0.53	0.30	0.06	4.8	33.5	60.0	1.92	
LHK	0.72	650	0.36	0.36	0.02	3.0	31.0	40.0	2.16	[23]
	0.76	500	0.40	0.38	0.015	2.0	29.5	40.0	2.13	
	0.78	300	0.50	0.39	0.01	2.0	22.0	20.0	2.06	

Table 2.
Model parameters of the CGMs used in the reviewed dams.

The nonlinear elasticity model proposed by Duncan and Chang [21] is properly among the most widely used constitutive models because of its simplicity in using and convenience of parameter determination. However, some important features cannot be captured by this model. For example, the model is proposed based on triaxial compression tests and the influence of the intermediate principal stress is not considered. Furthermore, the model is a nonlinear elasticity one that the shear-induced volumetric contraction and dilation cannot be reflected. Many advanced constitutive models have been proposed for soils within the framework of different theories in the past decades [24–27]. However, they are beyond the scope of this chapter and are not perused further.

4. Construction techniques

Natural impervious materials excavated from borrow areas usually do not meet the specified gradation requirements. For instance, the raw materials obtained in the PBG and CHB dams contain much oversize particles, which need to be sieved out before placement. On the contrary, the raw materials in the NZD and LHK dams contains too much fine particles that the deformation moduli are not high enough and certain contents of coarse gravel should be added. Therefore, the most frequently required operations in preparing the core materials are screening and blending. This section gives some experiences used in the four dams reviewed.

4.1 Screening

Oversize particles can be removed at the borrow area before loading using hand labor or on the fill surface after dumping by using special rock rakes [4, 8]. Both techniques are not of sufficient efficiency, and have not been used for the dams reviewed. The grizzly is the commonly used particle-separating device in the PBG and CHB dams. A grizzly is a grating made of heavy bars, across which the material to be processed is passed. The bars are wider at the top than at the bottom, so that
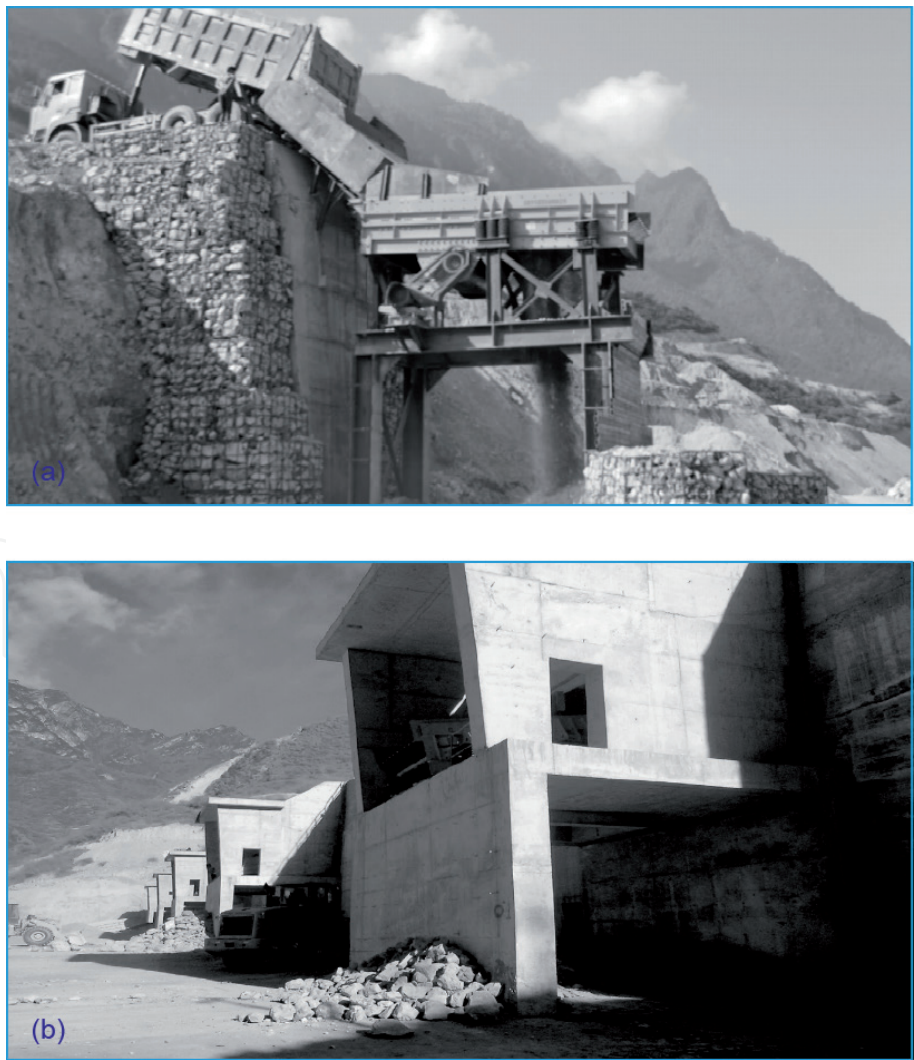

Figure 13.
Screening system for the CHB dam (at the courtesy of Xue K). (a) Test screening device and (b) five screening stations.

the openings between bars increase in width with depth and, therefore, are not easy to clog by particles caught partway through [4]. The grizzly is often constructed with a sloping, vibrating grating, so that oversize particles are dumped over the end of the grizzly, while the desired material passes through. **Figure 13(a)** shows a test grizzly built for the CHB dam. The raw material was dumped from the truck on a high platform and fed into the vibrating grating (frequency = 500–850 r/min) through a slope trough inclined at 35° (from the horizontal plane). The bars were spaced 150 mm and had a slight inclination of 5°. The amplitude of vibration was 6–10 mm. The simple device shown in **Figure 13(a)** was used initially, and later five screening stations (**Figure 13(b)**) were built following similar concepts to produce the required large amount of materials. In the screening stations, the inclination of the vibrating grating was increased to 10°, and bars 3.5 m in length were used without welding.

The screening system for the PBG dam is shown in **Figure 14**. The raw material was first dumped onto a sloped grizzly (opening = 300 mm, size = 4.5 m × 6.0 m, and inclination = 30–34°) to remove the particles larger than 300 mm. The soils passing through the grizzly was then transferred by a belt conveyor to a specifically fabricated shaking screen with the purpose of sieving out the particles larger than 80 mm. The resultant material was transferred by a belt conveyor to the dam site directly. Belt conveyors are most suitable for moving large quantities of material over rough terrain where there are large differences in elevation between the dam site and the borrow pits or screening stations [4]. In the current case, a special tunnel 4 m in width and 3 m in height was excavated (lined with concrete), in which the belt conveyor was installed. The difference in elevation of the inlet and outlet is 460 m and the horizontal distance is 3985.84 m, indicating an average slope angle of 6.6°. The 1000 mm wide belt had a speed of 4 m/s and was capable of conveying 1000 ton of screened material per hour.

Trommel is another kind of screening device suggested by U.S. Bureau of Reclamation [4], which sieve out the oversize particles by rotating a cylinder of perforated sheet metal or wire screen. This device has not been practiced in the reviewed cases. Interested readers are referred to the relevant design standard [4].

Figure 14.
Screening system for the PBG dam (at the courtesy of Yao FH).

4.2 Blending

For the NZD and LHK dams, the low content of gravel particles in the original materials excavated from borrow areas necessitates the addition of gravel fraction in order to increase the deformation moduli of the cores. The common blending practice used in both NZD and LHK dams may be simply described as *spreading horizontally and excavating vertically* as shown in **Figure 15**. For the NZD dam, a layer of gravel 50 cm in thickness was first spread. Then a layer of natural clay 110 cm in thickness was spread on the filled gravel layer [28]. Three such interlayers were placed, forming artificial horizontal soil strata. Power shovels with a bucket volume of 6 m^3 were subsequently used to excavate the soil strata vertically from the bottom as shown in **Figure 15**. Sufficient mixing was achieved by running the open bucket through the clay-gravel mixture several times before loading. The thickness of the gravel and clay layers for the NZD dam was intended to adding 35% of artificial gravel particles to the natural soils. For the LHK dam, 40% of gravel particles were required to mix with natural soils, and this was achieved by placing a 50-cm thick gravel layer and an 83-cm thick clay layer sequentially. Shovels with a bucket volume of 4 m^3 were used to excavate the prepared strata as shown in **Figure 15(b)**.

4.3 Compaction

Padfoot rollers were used to compact the CGMs used in the four rockfill dams without exception. The selection of compacting unit, the number of passes, and the loose lift thickness were based on test filling. **Table 3** summarizes the compaction parameters for the CGM used in the four ECRDs. Some important points deserves

(a)   (b)

Figure 15.
Blending techniques used in the NZD and LHK dams. (a) The NZD dam and (b) the LHK dam.

Dam	PBG	CHB	NZD	LHK
Loose lift thickness (cm)	45	30	27	30
Weight of compactor (ton)	25	26	22	26
Number of passes	8	2*+12	10	2*+10

*Note: *Number of passes of static compaction.*

Table 3.
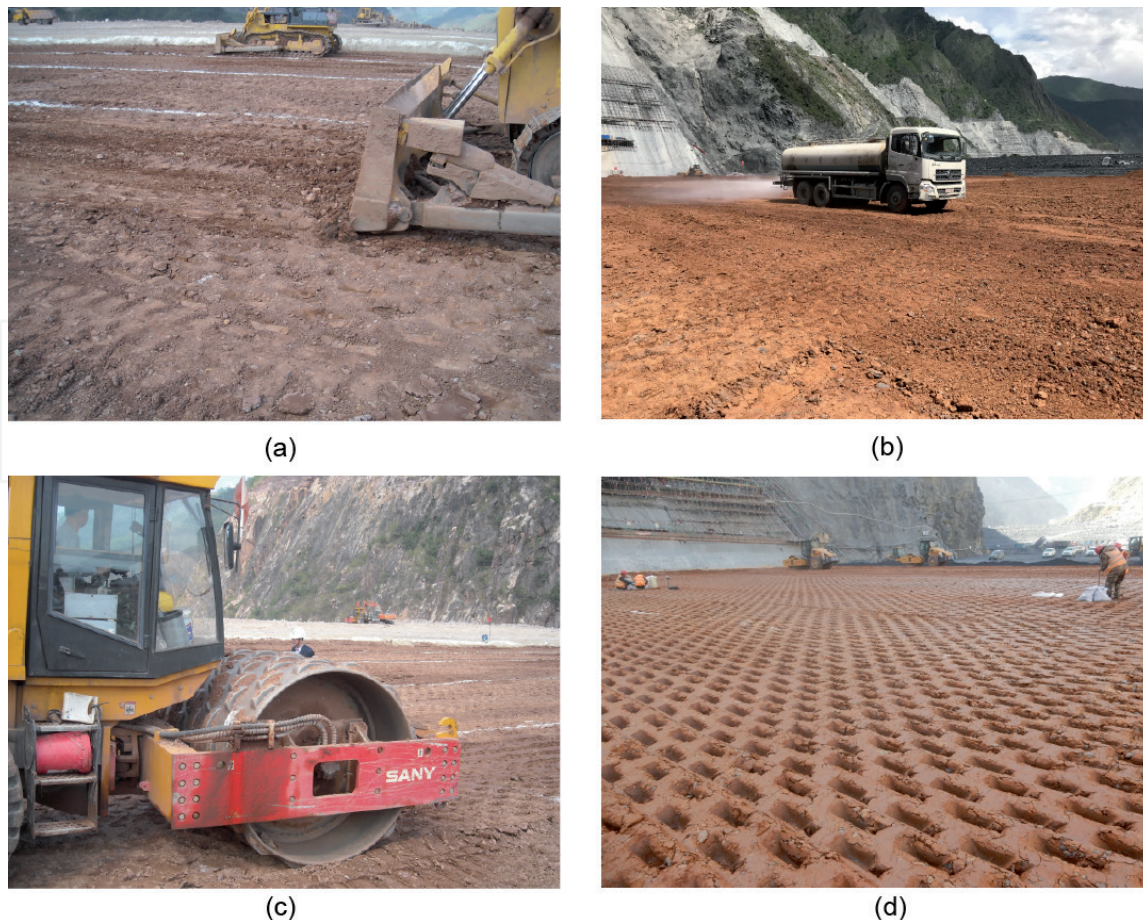*Roller compaction parameters for the CGMs.*

Figure 16.
Field compaction by GPS equipped padfoot rollers. (a) Scarification, (b) sprinkling, (c) compaction, and (d) quality checking.

to be mentioned. First, scarification of the surface of a compacted lift is always necessary prior to placing the next lift in order to ensure a good bond between the lifts. **Figure 16(a)** shows an example that scarification being performed by crawler tractors at the NZD dam. Second, the scarified loose surface layer may lose water due to evaporation, and watering the surface layer before placing the next lift is important. **Figure 16(b)** shows a truck sprinkling the surface of the LHK dam.

Strict compliance to the compaction specification is of great significance for a quality job. In the past two decades, global positioning system (GPS) technology has been increasingly used in dam engineering. GPS equipment has been carried by padfoot rollers in the NZD dam (**Figure 16(c)**) and later cases so that their routes of compaction and number of passes can be well monitored in the central control office. Once the action of a compaction roller deviates from the specification, remind or warn information can be send to the operator and immediate corrective measures can be taken. It is also important to note that blended soils generally have a wide grain size distribution. It is, therefore, necessary to perform quality checking more frequently to ensure that satisfactory results are obtained, as exemplified in **Figure 16(d)** taken from the LHK ECRD.

5. Field control test

Stability, deformation and seepage behaviors of ECRDs are generally evaluated using parameters obtained from laboratory and field tests where the samples are prepared at specified dry densities and water contents. This is the reason why soils

must be placed as specified; otherwise, design assumptions may not be met and, in the worst case, unexpected distress might occur in the finished structure. The basic properties that should be checked frequently for the compacted soils are the dry density and water content. The standards for percent of compaction and water content are usually established for the total material [1, 2], and this necessitates a certain number of large-scale compaction tests if the prototype CGM is to be tested as the largest particles are up to 75–150 mm in diameter (**Table 1**). It is, however, generally not feasible to do this because testing total material could not keep pace with the rate of fill placement. Therefore, rapid field control test methods should be devised to guarantee the compaction quality. In this part, some methods used in the reviewed ECRDs are introduced.

5.1 Method used for the NZD dam

The main difficulty in evaluating the degree of compaction for CGM is the time required to obtain its compaction curve. For instance, 8 hours were required to carry out the three-point rapid compaction tests with a mold 300 mm in diameter [2]. However, if the fine fraction (d < 20 mm in the case of NZD dam) was tested with a mold 152.4 mm in diameter, the volume of materials to be tested and the compaction effort can be reduced considerably and the rapid compaction tests can be finished within only 1 h. Therefore, it is natural to establish a relationship between the percent compaction of the total material and that of the fine fraction. The percent compaction specified for the CGM in the NZD dam is 95% [2], and the corresponding percent compaction of the fine fraction was established as follows:

1. Perform the standard five-point compaction tests for the total material with a modified Proctor compaction mold (diameter = 600 mm and effort = 2690 kJ/m^3) and find out the maximum dry density (ρ_{dmax}) and optimum water content (ω_{opt}) of the total material.

2. For the maximum dry density sample, sieve out the particles with diameters over 20 mm. Weigh the coarse particles (m_g) and evaluate the total volume (V_g) of these particles using the density of the gravel particles (ρ_g).

3. Assume that the total material was compacted to 95% of the maximum dry density, the total volume (V) of the sample can be evaluated as $V = m/(0.95\rho_{dmax})$ where m is the dry mass of the total material. The dry density of the fine fraction can then be evaluated by $\rho_c = (m–m_g)/(V–V_g)$.

4. Perform the standard five-point compaction tests for the fine fraction (d < 20 mm) with a standard Proctor compaction mold (diameter = 152.4 mm and effort = 595 kJ/m^3), and find out the maximum dry density (ρ^*_{dmax}) and optimum water content (ω^*_{opt}) of the fine fraction.

5. The percent compaction of the fine fraction can be calculated by ρ_c/ρ^*_{dmax}.

6. Repeat the above procedures for other contents of added gravel materials so that a reasonable range of percent compaction can be obtained for the fine fraction (d < 20 mm).

Figure 17 shows such a relationship established parallel by two companies. It has been found that the 95% of compaction for the total material (2690 kJ/m^3) can always be achieved when the fine fraction is compacted to 98% of its maximum dry

density (595 kJ/m^3). Therefore, this criterion was used in field to check the quality of compaction for the NZD dam. Only the dry density of the fine fraction needs to be calculated and the three-point rapid compaction tests were performed with the fine fraction.

The percent of compaction of the total material can be evaluated conveniently once its maximum dry density is known. Although this is time consuming and not practical in field, the maximum dry density of the total material can be evaluated a priori. For the NZD dam, the maximum dry densities of the total material with various contents of added gravel particles were obtained and plotted against P_{20} in **Figure 18**. Once the P_{20} after compaction is known, the maximum dry density and thus the percent compaction of the total material can be estimated using **Figure 18**. Both the percent compaction of the total material and that of the fine fraction were checked during the construction of the NZD dam. Back analyses using the pore water pressures measured by piezometers show that the permeability coefficient of the core material is of the magnitude of 10^{-9} cm/s, which is considerably lower than the values measured both in laboratory and in field [29].

5.2 Method used for the PBG dam

The maximum diameter of CGM in the PBG dam is 80 mm. Compaction criteria were specified for the fine fraction only ($d < 5$ mm), i.e., $\omega^* = \omega^*_{opt} + (1–2)\%$ and
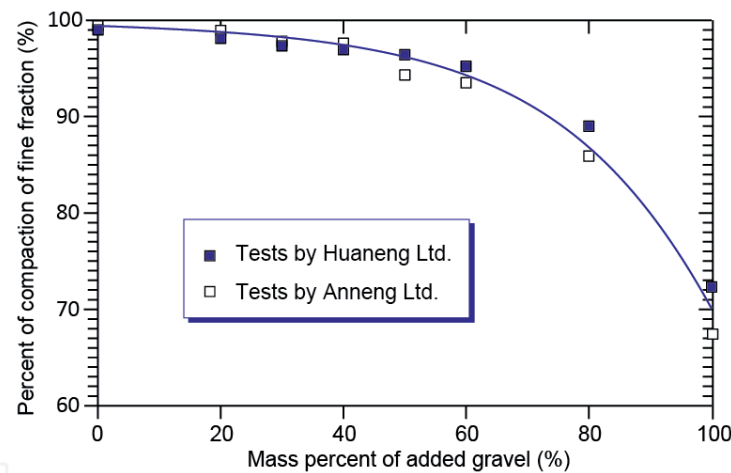

Figure 17.
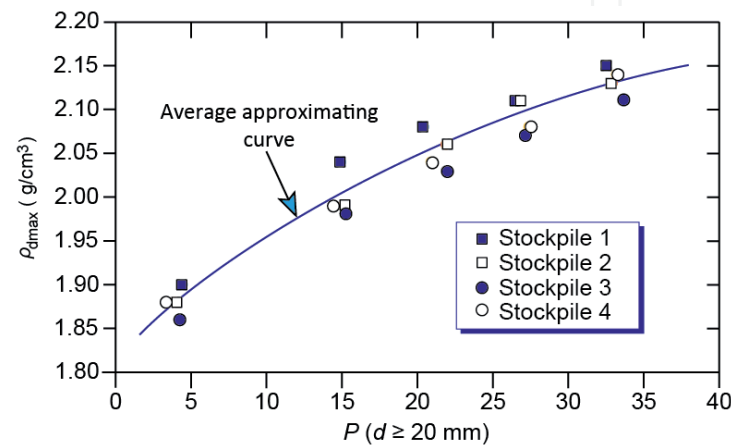*Percent of compaction of the fine fraction corresponding to 95% compaction of the total material.*

Figure 18.
Maximum dry density of total material with different P_{20}.

$\rho^*_d/\rho^*_{dmax} \geq 98\%$ (2740 kJ/m^3) or 100% (595 kJ/m^3). It is logical to perform three-point rapid compaction tests on fine fraction to check the criteria. However, an even simpler strategy was also used for the PBG dam. The procedure is described as follows. For a given dry density of the fine fraction (ρ^*_d), the relationship between the dry density of the total material (ρ_d) and the gravel content (c_g) is similar to Eq. (4) and Eq. (9), i.e.

$$\rho_d = \frac{\rho_g}{\left(1-c_g\right)\rho_g + c_g\rho^*_d}\rho^*_d \tag{17}$$

which is illustrated by the red curve in **Figure 19**. If the field water content of the total material (ω) is obtained, the wet density of the total material (ρ) at this water content can be estimated for each gravel content as illustrated by the blue curve in **Figure 19**. This blue curve is the border distinguishing the unacceptable samples from those acceptable ones. For instance, the sample denoted by point A has a wet density above the blue curve. This is realistic only when the dry density of the fine fraction is higher than ρ^*_d and thus the sample is acceptable. On the contrary, sample B has a wet density below the curve, indicating that its fine fraction has not been compacted to the dry density of ρ^*_d and therefore is unacceptable.

5.3 Method used for the CHB dam

Water content and gravel content are also important indices to be checked for the total material. For instance, determining the gravel content is the prerequisite of using the concepts given in **Figures 17** and **18**. However, evaluate the mass of water contained in the prototype material needs to dry the tested total material up to 8 h, and this is obviously not acceptable for a rapid check test. Bao et al. suggested a practical way to determine the water content and gravel content for the CHB dam [6, 7]. First, it is easy to verify that the water content of the total material (ω) can be calculated by the water content of the fine fraction (ω^*) and that of the gravel fraction (ω_g), that is

$$\omega = \left(1-c_g\right)\omega^* + c_g\omega_g \tag{18}$$

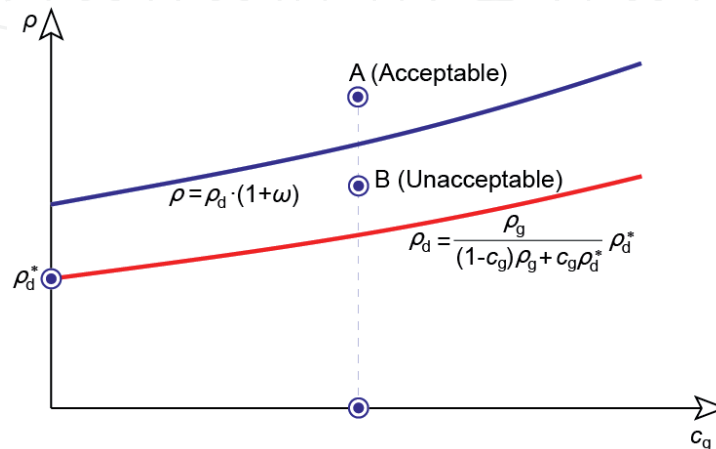in which c_g is again the mass percent of gravel particles (dry materials).

Figure 19.
Relationship between the wet density and gravel content.

Now assume that a test pit has been excavated and the total volume (V) of the pit has been obtained by filling water or sand. The total wet mass of the excavated materials (M) can also be obtained immediately. The total material is then sieved into two parts, i.e., the gravel particles ($d \geq 5$ mm) and the fine fraction ($d < 5$ mm). The sample of fine fraction can be dried quickly by open alcohol flame, and the water content (ω^*) is easily obtained. Meanwhile, the sieved gravel particles are washed with clean water and wiped with dry towels. The wet mass of these clean gravel particles (M_g) are weighed as soon as possible. The wet mass of the fine fraction (M_c) can now be determined as $M_c = M - M_g$. Consequently, the dry mass of the fine fraction (m_c) is obtained, i.e.

$$m_c = \frac{M_c}{1 + \omega^*} \tag{19}$$

The key assumption adopted by Bao et al. is that all the gravel particles are in a saturated state with dry surfaces. This water content is normally in the range of 1.5–3.5%, with an average of 2.3% in the CHB case. With this average value for ω_g, the dry mass of the gravel particles (m_g) can be readily obtained, i.e.

$$m_g = \frac{M_g}{1 + \omega_g} \tag{20}$$

The mass content of the gravel content is calculated by $c_g = m_g/(m_g + m_c)$, and the water content of the total material can be estimated by Eq. (18). The volume of the gravel particles (V_g) can either be measured directly or be calculated using its wet mass and apparent wet density [6, 7]. Afterward, the volume of fine fraction (V_c) is obtained as $V_c = V - V_g$. Then, the dry density of the total material (ρ_d) and the fine fraction (ρ^*_d) can be obtained as follows:

$$\rho_d = \frac{m_c + m_g}{V}, \quad \rho^*_d = \frac{m_c}{V_c} \tag{21}$$

This rapid method can be used to assess the compaction quality for both the total material and the fine fraction. However, two aspects need to be pointed out. First, the fine fraction is dried by alcohol flame, which can result in inaccuracy in water content because the high temperature applied to the soil can drive off the adsorbed water and burn or drive off volatile organic matter, neither of which should be removed in a normal water content test [30]. Second, the water content assumed for the gravel particles may influence the results to an unacceptable level. Preliminary check tests should be performed before using. **Figure 20** compares the water contents of total material samples obtained by alcohol flaming and normal oven drying as well as the gravel contents obtained by two methods. The difference in water content by the two methods varies in the range of –0.6–0.6%, with an average of –0.1%, indicating the reliability of the flaming method for this particular case. Furthermore, the gravel contents obtained by the two methods are also very close to each other with a slight difference ranging between –0.4 and 0.3%.
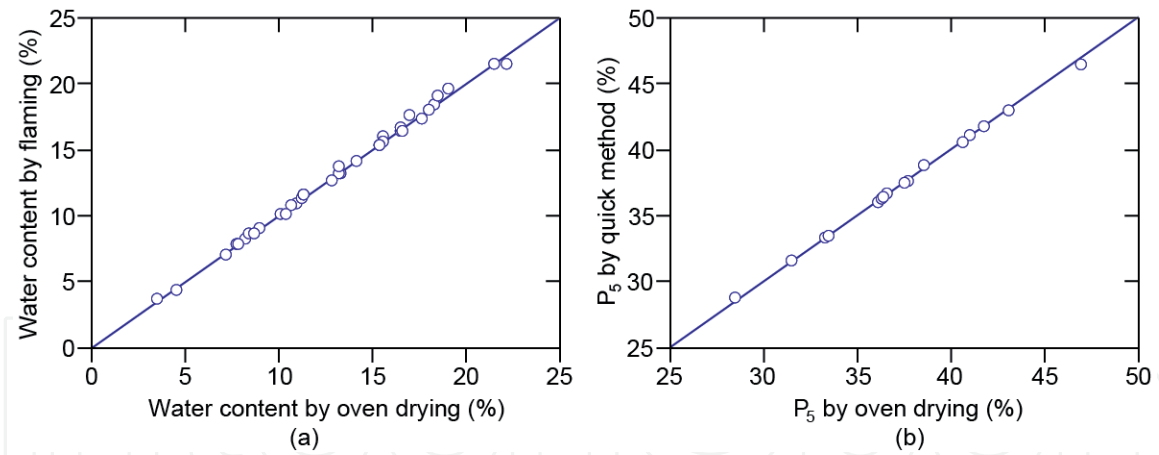
Figure 20.
Verification of the method used in the CHB dam. (a) Water content verification and (b) gravel content verification.

Two aspects are concerned as can be summarized from the above cases, i.e., the degree of compaction of the total material and that of the fine fraction (the diameter defining the fine fraction varies from dam to dam, e.g. 20 mm in the NZD dam and 5 mm in the CHB dam). The percent compaction of the total material is useful to guarantee the overall deformation performance but is not enough to ensure the impermeability of the fine fraction. On the other hand, the percent compaction of the fine fraction is a good indication of the impermeability but is not enough for the overall behavior of the total material. The concept of quality control for high ECRDs is increasingly stringent. For the PBG dam, emphasis was placed on the fine fraction. For the NZD dam, three-point rapid compaction tests were performed to check the compaction quality of the fine fraction ($d < 20$ mm). The percent compaction of the total material was not checked every point but was checked periodically. For the CHB dam, both the percent of compaction of the total material and the fine fraction were checked simultaneously, and this concept is used similarly in the LHK ECRD under construction. Deformation and seepage behaviors of these dams monitored in field prove the effectiveness of these control test methods.

6. Conclusions

Clay and gravel mixture has been used in constructing impermeable system of embankment dams for many years. The compaction performance as well as the strength, deformation and permeability behaviors are considerably influenced by the quantity of gravel contained. Determining and controlling the gravel content is therefore of great significance in design and construction. Many compaction tests performed for the reviewed cases in this chapter show that the fine fraction can be compacted to its densest state when the gravel content is below about 30%, beyond which the maximum dry density of the total material continues to increase while the percent compaction of the fine fraction decreases, as evidenced by the abrupt increase in permeability. A peak for the maximum dry density of the total material can generally be achieved when the gravel content is around 70%, beyond which the dry density decreases considerably when the gravel content is further increased.

Removing oversize particles from a cohesive soil is generally not easy, especially when the soil is in a wet state. However, experience obtained previously shows the success of using slope grizzlies and some shaking /vibrating screens or both. When a certain amount of gravel is to be blended with a raw material, the spreading and excavation practice seems to be an effective way. Scarification, sprinkling, and field

checking should be performed to ensure the compaction and bonding quality and confirm the design assumptions. It is now a trend that both the percent compaction of the fine fraction and that of the total material be verified using some rapid field control tests as exemplified in this chapter.

Properties that have not been discussed but are also very important to the safety of embankment dams include the dynamic behavior, wetting-induced collapse behavior, and creep behavior of clay and gravel mixtures. Laboratory tests have been performed and various constitutive models that describing these important behaviors have been proposed and incorporated into finite element procedures, which play important role in predicting the performance of dams to be built. Field instrumentations for settlement, earth pressure and pore water pressure have also provided valuable information on the safety status of constructed dams. All these advances have contributed to the successful construction and operation of the reviewed cases and will continue to play important roles in even higher earth and rockfill dams.

Acknowledgements

Author details

Zhongzhi Fu*, Shengshui Chen, Enyue Ji, Guoying Li and Yang Lu
Geotechnical Engineering Department, Nanjing Hydraulic Research Institute, Nanjing, China

*Address all correspondence to: fu_zhongzhi@yahoo.com

IntechOpen

References

[1] China Ministry of Water Resources. Design Specification for Rolled Earth-Rock Fill Dams (SL 274-2001). Beijing: China Water & Power Press; 2011

[2] Zhang ZL. Key Technologies for Earth Core Rockfill Dams Higher Than 200 m and Their Engineering Application. Beijing: China Water & Power Press; 2011. ISBN: 978-7-5084-4447-5

[3] USBR (U.S. Bureau of Reclamation). Chapter 2: Embankment design. In: Design Standards No. 13 Embankment Dams. Denver; 2012

[4] USBR (U.S. Bureau of Reclamation). Chapter 10: Embankment construction. In: Design Standards No. 13 Embankment Dams. Denver; 2012

[5] Yao FH, Yang XG. Key Technologies in PuBuGou Gravely Earth Core Rockfill Dam. Beijing: China Water & Power Press; 2015. ISBN: 978-7-5170-3293-9

[6] Bao HF, Wang HB, Pang G, Wang K. Research on rapid detection method for filling quality of impervious core wall with gravelly soil in dam. Journal of Water Resources and Architectural Engineering. 2014;**12**(1):105-111. DOI: 10.3969/j.issn.1672-1144.2014.01.022

[7] Bao HF, Pang G, Yang YB, Hu P. Study on the compaction characteristics and maximum dry density of gravel soil. Geotechnical Investigation and Surveying. 2016;**9**:22-28

[8] Xue K, Liu XS, Yao KW. Techniques used in removing oversize particles in the gravely soils used in the ChangHeBa hydropower station. Sichuan Water Power. 2015;**34**(3):25-30. DOI: 10.3969/j.issn.1001-2184.2015.03.006

[9] Zhang ZL, Feng YL, Xiang B, Yuan YR. Design, researches and practices of impervious materials for core wall of Nuozhadu Hydropower Station. Chinese Journal of Geotechnical Engineering. 2013;**35**(7):1323-1327

[10] Xiong L, Yang JP. Sensitivity analysis of the mixing parameters for the clay gravel mixtures used in the LiangHeKou dam and the controlling measures. Construction of Water Conservancy and Hydropower Engineering. 2017;**5**:62-66

[11] Che WB, Yang JP, Jiang WH, Chen X. Analysis on roller compaction tests of gravel soil material in LiangHeKou hydropower station. Water Power. 2018;**44**(2):28-32. DOI: 10.3969/j.issn.0559-9342.2018.02.008

[12] Lu Y. Experimental study and mechanism analysis of engineering properties of clay mixed with gravel under cold environments [thesis]. Nanjing: Hohai University; 2019

[13] ASTM. Standard Test Methods for Laboratory Compaction Characteristics of Soil Using Standard Effort (D 698-00). West Conshohocken; 2000

[14] ASTM. Standard Test Methods for Laboratory Compaction Characteristics of Soil Using Modified Effort (D 1557-02). West Conshohocken; 2002

[15] Shelley TL, Daniel DE. Effect of gravel on hydraulic conductivity of compacted soil liners. Journal of Geotechnical Engineering. 1993;**119**(1):54-68

[16] ASTM. Standard Test Method for Infiltration Rate of Soils in Field Using Double-Ring Infiltrometer (D 3385-03). West Conshohocken; 2003

[17] Lambe TW. The engineering behaviour of compacted clay. Journal of Soil Mechanics and Foundations Division. 1958;**84**(2):1-35

[18] Mitchell JK, Hooper DR, Campanella RG. Permeability of compacted clay. Journal of Soil Mechanics and Foundations Division. 1965;**91**(4):41-65

[19] Alonso EE, Pinyol NM, Gens A. Compacted soil behavior: Initial state, structure and constitutive modelling. Géotechnique. 2013;**63**(6):463-478. DOI: 10.1680/geot.11.P.134

[20] Sivakumar V, Wheeler SJ. Influence of compaction procedure on the mechanical behaviour of an unsaturated compacted clay. Part 1: Wetting and isotropic compression. Géotechnique. 2000;**50**(4):359-368

[21] Duncan JM, Chang CY. Nonlinear analysis of stress and strain in soils. Journal of Soil Mechanics and Foundations Division, ASCE. 1970;**96**(5):1629-1653

[22] Xiong K, He YL, Wu XY, Dong YL. Stress and deformation behavior of foundation gallery of ChangHeBa hydropower station. Chinese Journal of Geotechnical Engineering. 2011;**33**(11):1767-1774

[23] Chen ZB, Zhu JG. Three-dimensional finite element analysis on stress-strain and materials parameters sensibility of LiangHeKou core rockfill dam. Journal of Fuzhou University (Natural Science). 2010;**38**(6):893-899

[24] Huang MS, Yao YP, Yin ZY, Liu EL, Lei HY. An overview on elementary mechanical behaviors, constitutive modeling and failure criterion of soils. In: Proceedings of the 12th National Conference on Soil Mechanics and Geotechnical Engineering; Engineering. Shanghai; 17-21 July 2015. pp. 1-26

[25] Kolymbas D. An outline of hypoplasticity. Archive of Applied Mechanics. 1991;**61**:143-151

[26] Zienkiewicz OC, Chan AHC, Pastor M, Schrefler BA, Shiomi T. Computational Geomechanics with Special Reference to Earthquake Engineering. New York: John Wiley & Sons; 1999

[27] Fu ZZ, Chen SS, Wei KM. A generalized plasticity model for the stress-strain and creep behavior of rockfill materials. Science China Technological Sciences. 2019;**62**:1-19. DOI: 10.1007/s11431-018-9362-3

[28] Wang YF, Chi X. Techniques for blending clay-gravel mixtures for 300-m extremely high rockfill dams. Construction and Maintenance of Water Project. 2018;**9**:5-10. DOI: 10.16616/j.cnki.11-4446/TV.2018.09.02

[29] Wu YK, Zhang BY, Yu YZ, Zhang ZL. Consolidation analysis of NuoZhaDu high earth-rockfill dam based on the coupling of seepage and stress-deformation-physical state. International Journal of Geomechanics. 2016;**16**(3):1-11. Article No: 04015085. DOI: 10.1061/(ASCE)GM.1943-5622.0000555

[30] USACE (U.S. Army Corps of Engineers). Construction control for earth and rock-fill dams. In: Engineering Manual. EM 1110-2-1911. Washington, DC; 1995